Long-term evolution of the three-dimensional structure of string-fluid complex plasmas in the PK-4 experiment

S. Mitic [1,*] M. Y. Pustylnik,[1] D. Erdle,[1] A. M. Lipaev,[2] A. D. Usachev,[2] A. V. Zobnin,[2] M. H. Thoma,[4] H. M. Thomas [1] O. F. Petrov,[2,3] V. E. Fortov,[2,†] and O. Kononenko[5]

[1]*Institut für Materialphysik im Weltraum, Deutsches Zentrum für Luft- und Raumfahrt (DLR), Münchener Straße 20, 82234 Weßling, Germany*
[2]*Joint Institute for High Temperatures, Russian Academy of Sciences, Izhorskaya ul. 13/19, 125412 Moscow, Russia*
[3]*Moscow Institute of Physics and Technology, Institutsky lane 9, 141700 Dolgoprudny, Moscow Region, Russia*
[4]*I. Physikalisches Institut, Justus-Liebig-Universität Gießen, Heinrich-Buff-Ring 16, 35392 Gießen, Germany*
[5]*Gagarin Research and Test Cosmonaut Training Center, 141160 Star City, Moscow Region, Russia*

Microparticle suspensions in a polarity-switched discharge plasma of the Plasmakristall-4 facility on board the International Space Station exhibit string-like order. As pointed out in [Phys. Rev. Research **2**, 033314 (2020)], the string-order is subject to evolution on the timescale of minutes at constant gas pressure and constant parameters of polarity switching. We perform a detailed analysis of this evolution using the pair correlations and length spectrum of the string-like clusters (SLCs). Average exponential decay rate of the SLC length spectrum is used as a measure of string order. The analysis shows that the improvement of the string-like order is accompanied by the decrease of the thickness of the microparticle suspension, microparticle number density, and total amount of microparticles in the field of view. This suggests that the observed long-term evolution of the string-like order is caused by the redistribution of the microparticles, which significantly modifies the plasma conditions.

I. INTRODUCTION

The Plasmakristall-4 (PK-4) [1] laboratory is a presently operational complex plasma facility on board the International Space Station (ISS). It is a continuation of the research program started by such experiments as PKE-Nefedov [2] and PK-3 Plus [3]. Complex plasmas [4–7] are used as models for particle-resolved studies of generic classical condensed-matter phenomena. Since complex plasmas contain micron-sized solid microparticles (along with electrons, ions, and neutral molecules), the microgravity is necessary to create unperturbed three-dimensional (3D) suspensions of microparticles: Under ground laboratory conditions, the microparticles concentrate themselves at the bottom edge of the plasma, where the gravitational force can be compensated by the electrostatic force due to the large sheath electric field [8]. In the framework of the microgravity research program on the ISS, such generic phenomena such as freezing and melting transitions [9–13], shock waves [14], lane formation [15,16], shear flow [17], etc. were investigated in 3D complex plasmas under long-term microgravity.

Another phenomenon which attracted the attention of complex plasma researchers is electrorheology [18–21]. "Conventional" electro- [22,23] or magnetorheological fluids [24,25] consist of suspensions of microparticles in nonconducting fluids. They can drastically change their viscosity upon the application of external electric or magnetic fields.

The external field polarizes (magnetizes) the microparticles and induces additional dipole coupling between them. Microparticles start to form strings in the direction of the induced dipoles. In complex plasmas, the electric field can polarize the shielding ion cloud around the microparticles. Therefore, the microparticles in complex plasmas may be subject to the same string-formation phenomenon as microparticles in conventional electrorheological fluids. This phenomenon was observed in PK-4 in the polarity-switched DC discharge [19] as well as in a combined rf and DC discharge [26].

In the presence of the fast oscillating electric field (use of DC electric fields is impractical because of the drift of the charged microparticles and instabilities they cause [19,27]), the interaction potential of the microparticles can be represented as a superposition of the following two terms [18,28]: the Yukawa term

$$\phi_Y = \frac{Q_d^2}{4\pi\epsilon_0 d} \exp\left(-\frac{d}{\lambda}\right), \tag{1}$$

where Q_d is the microparticle charge, d is the interparticle distance, λ is the Debye screening length; and the quadrupole term that for the collisionless case can be written as

$$\phi_Q = -0.43 \frac{Q_d^2}{4\pi\epsilon_0 d} \frac{M^2\lambda^2}{d^2}(3\cos^2\zeta - 1), \tag{2}$$

where M is the thermal Mach number of the ion flow and ζ is the angle formed by the vector connecting the two microparticles and the external electric field.

Recently, using the data obtained in one of the PK-4 experiments, we have obtained 3D structure of string-fluid complex

plasmas [20]. Structural analysis was performed using the 3D pair correlations and the length spectrum of string-like clusters (SLCs). Also, the long-term evolution of the 3D structure in the suspension was observed. In the continuation of that work, in this paper, we perform the detailed analysis of the long-term evolution. We investigated the dependence of the observed order on the thickness of the microparticle cloud, microparticle number density, and the total number of microparticles.

The paper is organized as follows: In Sec. II, we describe the experimental setup. In Sec. III, we explain the methods of data analysis used in the work. In Sec. IV, we show our experimental results and discuss them in Sec. V. Section VI concludes the paper.

II. EXPERIMENTAL SETUP

Experiments were performed in the flight model of PK-4 microgravity complex plasma facility on board the ISS [1]. In PK-4, a DC discharge plasma (with the maximal current of 3 mA) is produced inside a glass tube of 3 cm diameter. Polarity of the discharge can be switched with the frequency of up to several kHz. Gas pressure can be varied in the range of 0.1–2 mbar. Monodisperse melamineformaldehyde microspheres (of different diameters) can be injected into the plasma chamber using the dispensers, transported into and trapped in the working area. In the working area, the suspension of microparticles gets illuminated by a laser sheet and can therefore be observed by video cameras.

We used the same experimental procedure as in Ref. [20]. The microparticles of 3.34 μm diameter were injected into the DC discharge in argon with the current of 0.5 mA. As the microparticles arrived into the field of view, they got trapped by a polarity-switched discharge with the frequency of 500 Hz and 0.5 mA current. The trapped microparticle suspension was scanned in the direction perpendicular to the image. For this, the cameras and the laser optics were synchronously moved to keep the plane of the laser sheet always in the focus of the cameras. The scanning speed of $v_{scan} = 0.9$ mm/s results in about 15 μm separation between the consecutive frames along the scan direction. Four scans with the time interval of approximately two minutes between them were performed. The entire procedure was repeated for each of the two different argon pressures of 0.28 and 0.6 mbar. Only the video data from camera 1 were used in this work. The size of the field of view was 1600×600 pixels. The field of view was centered on the axis of the plasma chamber.

From the scan data, we were able to reconstruct the 3D structure of the microparticle suspension. For that, we traced the microparticles from frame to frame. Each detected trajectory corresponded to a microparticle, whose position was determined by weighting the trajectory with the integral intensity of a microparticle image in every frame. Some trajectories got unphysically long since they contained overlapped trajectories of more than one microparticle. For those trajectories, minima of microparticle image intensity were used as boundaries between the parts of a trajectory corresponding to different microparticles. Such a long trajectory was therefore accordingly split into pieces. Each piece was then treated as an independent trajectory corresponding to a
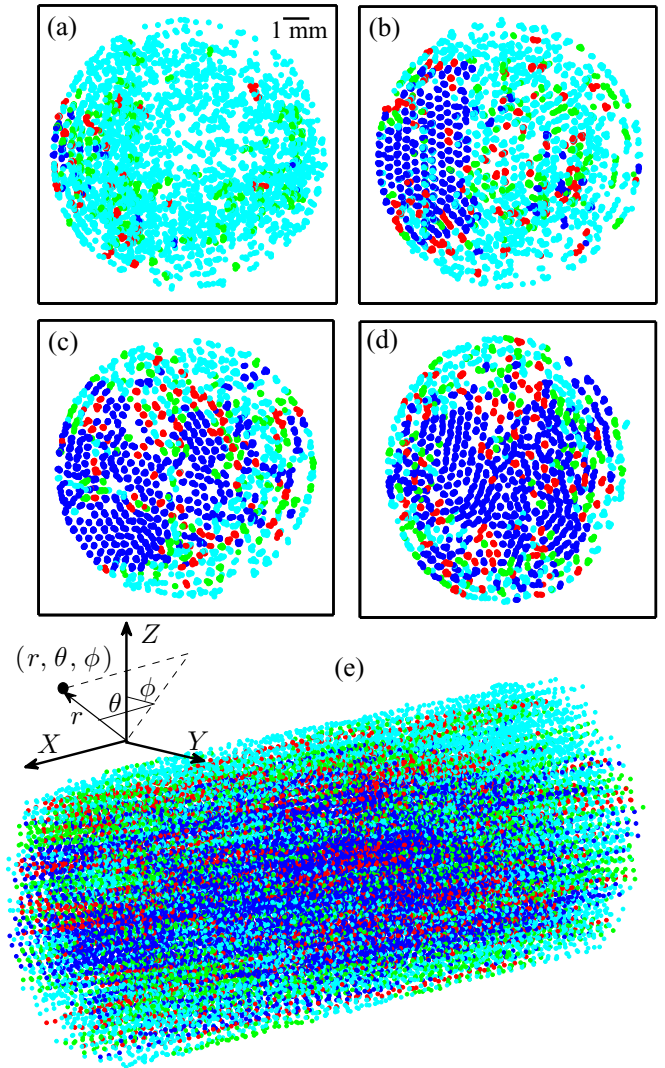

FIG. 1. Examples of the reconstructed microparticle suspensions consisting of 3.34-μm-diameter microspheres in the DC discharge at 0.28 mbar argon pressure with 0.5 mA current, polarity switching frequency 500 Hz: (a)–(d) Views along the axis of the plasma chamber onto the central transverse slices of 2 mm thickness for scans 1 to 4, respectively. (e) Fully reconstructed 3D structure of a microparticle suspension for scan 4. The microparticles are color coded according to the length of the strings they belong to. The blue domain indicating the strings with more than 20 microparticles is growing from scan 1 to scan 4. The transverse slices exhibit hexagon-like order of the strings. Also, the diameter of the slice is slightly decreasing with scan number. The X axis corresponds to the axis of the plasma chamber, the (X, Z) plane is the image plane of the cameras, and the Y axis is the scan direction. In panels (a)–(d), the microparticles are color coded according to the length of the string-like cluster *l* they belong to in the following way: 3–10: cyan, 10–15: green, 15–20: red, ⩾20: blue.

single microparticle. Examples of the reconstruction of the 3D structure of microparticle suspensions are shown in Fig. 1. The unphysically long trajectories were nonuniformly distributed in the suspension. Their fraction drastically increased in the direction of the X axis [Fig. 1(e)] at about 7 mm from

the right edge of the field of view. The reason for this increase is the respective spatial growth of the laser sheet width.

III. DATA ANALYSIS

For the structural analysis, we used the instruments that were found to be appropriate for the analysis of string-like order in Ref. [20]. Integrals of the pair correlation function

$$G(r, \theta, \phi) = \frac{1}{n_d N} \sum_{i,j=1 \ i \neq j}^{N} \frac{\delta(r_{ij} - r)\delta(\theta_{ij} - \theta)\delta(\phi_{ij} - \phi)}{4\pi r^2 \cos\theta},$$

(3)

where r, θ, and ϕ are the current spherical coordinates [see Fig. 1(e)], r_{ij}, θ_{ij}, and ϕ_{ij} are the length, polar angle, and azimuthal angle of a vector connecting microparticles i and j, N is the number of microparticles, n_d is the macroscopic microparticle number density, and

$$G_\phi(r, \theta) = \int_0^{2\pi} G(r, \theta, \phi) d\phi$$

(4)

and

$$G_\theta(r, \phi) = \int_{-\frac{\pi}{2}}^{\frac{\pi}{2}} G(r, \theta, \phi) \cos\theta d\theta$$

(5)

were used for the qualitative characterization of order. We checked the effect of unphysically long microparticle trajectories observed during scans on the pair correlations by comparing $G_\phi(r, \theta)$ and $G_\theta(r, \phi)$ calculated separately in the rightmost 7 mm of the field of view and in the rest of the suspension. No spurious correlation features produced by the unphysically long microparticle trajectories were found.

Detection of string-like clusters (SLCs) was done in the following way: First, for each microparticle m in the suspension, we found the so-called string neighbors, i.e., such neighbors n for which the distance r_{mn} and angle θ_{mn} lie inside the main string peak of G_ϕ [20]. Then, microparticles were grouped into SLCs using the friend-of-friends algorithm [9]. The length of a SLC l was determined as the number of microparticles belonging to it. We calculated the SLC length spectrum $S(l)$ as the number of SLCs for each length normalized by the total number of identified microparticles so that

$$\sum_{l=1}^{l_{max}} S(l)l = 1,$$

(6)

where l_{max} is the maximal detected SLC length.

IV. EXPERIMENTAL RESULTS

Figures 2(a) and 2(b) show the examples of G_ϕ and G_θ for 0.28 and 0.6 mbar, respectively. For both pressures, string-like order is manifested by the series of peaks in the vicinity of $\theta = \pm\pi/2$. In the following, we call these peaks the *string peaks*. Also, for both pressures, the arch-shaped features with the minimum of r at $\theta = 0$ responsible for the interstring correlations are visible. In the following, we call this feature the *interstring arch*. Unlike Ref. [20], the interstring arch exhibits a series of clear peaks, which means that axially aligned
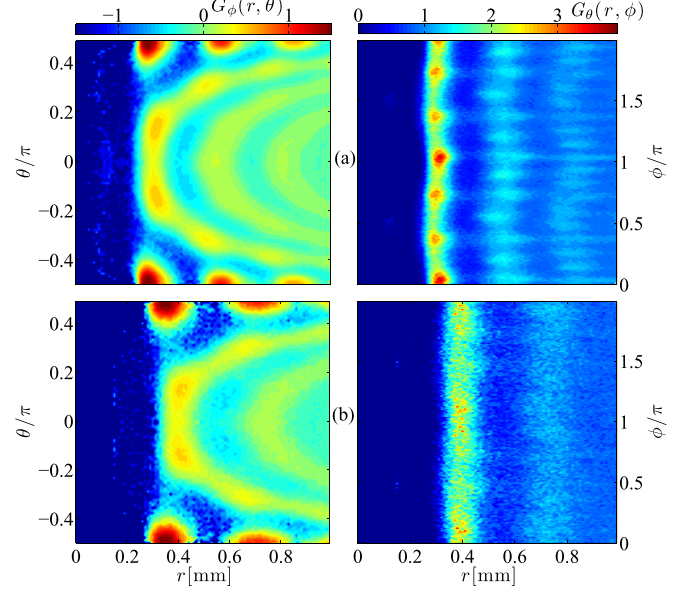

FIG. 2. Pair correlation functions $G_\phi(r, \theta)$ and $G_\theta(r, \phi)$ for the suspensions consisting of 3.34-μm-diameter microparticles in the DC discharge with 0.5 mA current and pressure and polarity switching frequency of 500 Hz at pressures of (a) 0.28 mbar and (b) 0.6 mbar. Distributions are shown for scan 4 representing the best order achieved at each pressure, respectively. The string peaks in $G_\phi(r, \theta)$ manifest the order inside the SLCs. The interstring arch exhibits several peaks, suggesting the rudiments of hexagonal structure. Equidistant peaks in $G_\theta(r, \phi)$ at 0.28 mbar manifest the hexagonal arrangement of SLCs in the azimuthal direction. The broad peaks in $G_\theta(r, \phi)$ at 0.6 mbar are supposed to be artifacts of disturbance of correlations caused by scanning and jerky drift of microparticles.

SLCs also exhibit a certain arrangement with respect to each other. The two nearest neighbors of a microparticle belonging to a neighboring SLC are aligned approximately along $\theta = \pm\pi/6$, which suggests that the interstring correlations contain the rudiments of hexagonal order. This is also true for both pressures.

The azimuthal order is, however, very different for two pressures. At 0.28 mbar [Fig. 2(a)], G_θ exhibits six clear equidistant peaks in the first coordination sphere. In the second coordination sphere, more frequent peaks are observed. We note that, even in slices in Figs. 1(a)–1(d), where not all the microparticles are shown, the hexagonal cells are easily seen.

At 0.6 mbar [Fig. 2(b)], the situation is different. The suspension does not exhibit any regular azimuthal structure except for two quite broad maxima at $\phi = 0$ and $\phi = \pi$. The direction determined by these angles coincides with the Z axis [Fig. 1(e)], which is parallel to the image plane. As also pointed out in Ref. [20], the microparticle suspensions experiences jerky axial drift with the average velocities of -0.2 mm/s for 0.6 mbar and 0.07 mm/s for 0.28 mbar. Therefore, the correlations in microparticle positions obtained by scanning with the velocity of 0.9 mm/s, will be affected by the scan in all the directions, which do not lie in the image plane. We suppose therefore that the broad angular maxima in G_θ at 0.6 mbar are unphysical and represent an artifact of
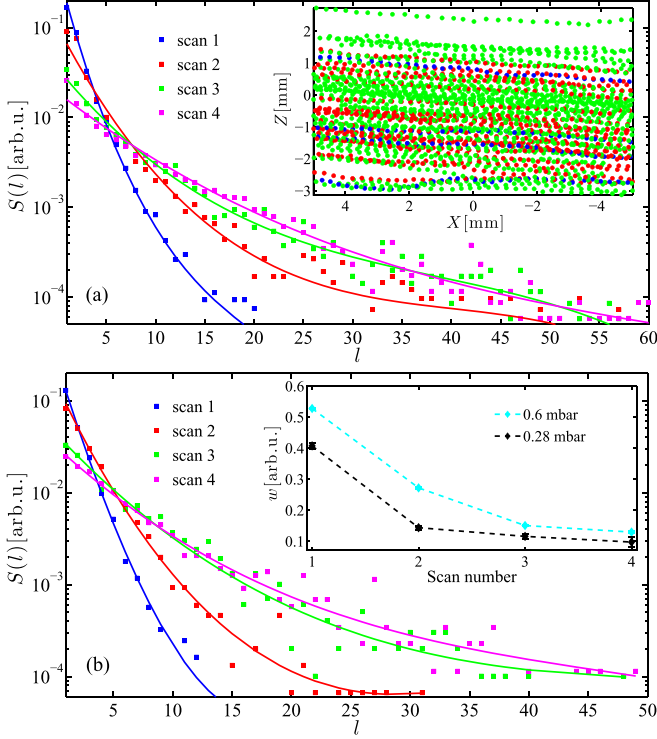
FIG. 3. Measured SLC length spectra $S(l)$ of the microparticle suspensions consisting of 3.34 μm microspheres in an argon DC discharge with 0.5 mA, polarity switching frequency 500 Hz, and at pressures of (a) 0.28 and (b) 0.6 mbar, and their fits [Eq. (7)]. The inset to panel (a) shows the selection of SLCs detected in scan 4 at 0.28 mbar. The SLCs are color coded by their length l in the following way: 40–50: green, 50–60: red, $\geqslant$60: blue. The inset to panel (b) shows the evolution of the average decay rate of the spectrum [given by Eq. (8)] from scan to scan. Time interval between the scans is approximately 2 minutes.

scanning. A similar effect is observed at 0.28 mbar [Fig. 2(a)], where two hexagonal peaks of G_θ located close to $\phi = 0$ and $\phi = \pi$ have higher intensity than the remaining four.

SLC length spectra are shown in Fig. 3. The spectra can be well fit with the function

$$S_{\mathrm{f}}(l) = S_0 \exp\left[P(l)\right], \quad (7)$$

where the polynomial $P(l) = al^3 + bl^2 + cl$. Third-order representation of $P(l)$ was the lowest-order representation which allowed for the adequate fit of the experimental SLC length spectrum. The average logarithmic derivative

$$w = -\left\langle \frac{1}{S_{\mathrm{f}}(l)} \frac{\partial S_{\mathrm{f}}(l)}{\partial l} \right\rangle_{1 \leqslant l \leqslant l_{\max}} = \frac{P(1) - P(l_{\max})}{l_{\max} - 1} \quad (8)$$

determines the average decay rate of the spectrum and can therefore be used as a measure of order in the microparticle subsystem. Increase of w corresponds to the decrease of string order. We note that, in Ref. [20], $P(l)$ contained only the linear term. In that case, however, $l_{\max}$ was limited to 11, whereas in the present work it is always as large as several tens, reaching 62 for scan 4 at 0.28 mbar.

The inset to Fig. 3(b) shows the monotonic decrease of the SLC spectrum decay rate w from scan to scan. Since the

externally controlled discharge parameters (pressure, current, polarity switching frequency, and duty cycle) were kept constant, the observed structural changes can only be connected with the locally observed parameters of the microparticle suspension varying due to, e.g., slow axial drift. Small change in the transverse dimensions of the microparticle suspension between the scans (also reported in Ref. [20]) can be seen in Figs. 1(a)–1(d).

In Fig. 4, we tried to identify the correlation of w with such parameters of the microparticle suspension in the field of view as the radius of the transverse cross section of the microparticle suspension R [Fig. 4(a)], average number density of microparticles n_{d} [Fig. 4(b)], and the total number of microparticles N [Fig. 4(a)]. For both pressures, w was found to grow with R, n_{d}, and N with the only exception being for the interval between the third and fourth scan in Fig. 4(b). This confirms the observation of Ref. [20], where better string order was found for a thinner suspension.

V. DISCUSSION

Peaks in the interstring arch as well as the azimuthal structure in Fig. 2(a) suggest that our suspensions exhibit some crystalline features. Together with Fig. 1, this suggests the formation of crystalline domains in the late scans. Deeper analysis might reveal the respective lattice types. However, since in $G_\phi(r, \theta)$, the main correlations are concentrated in the string peaks, this structure cannot be termed an anisotropic crystal. It is not only slightly compressed in the direction of the oscillating electric field (Fig. 2). It is much more probable to find a neighbor of a microparticle in this direction rather than in other (crystalline) directions. Therefore, we suppose the observed structure can still be discussed in terms of axially extended quasi-one-dimensional SLCs.

Degradation of the string order with the increase of the radial extension, microparticle number density and total amount of microparticles at constant externally controlled parameters suggests the crucial role of microparticle-plasma interactions. Indeed, the expression for the quadrupole term of the microparticle interaction potential [Eq. (2)] is derived for a single microparticle in a plasma with the ion flow [28] and only implies presence of the ion flow with a certain Mach number M. The ion flux is driven by the axial electric field. In a DC discharge, the same axial electric field accelerates the plasma electrons to energies which allows the ionization of the neutral atoms.

In a microparticle-free discharge, the ionization is balanced by the diffusion of the plasma to the walls of the plasma chamber. It was shown in many publications [29–32] that, in the case when a discharge contains significant amounts of microparticles, ionization balance inside the microparticle suspension becomes local. For the case of a DC discharge, it was shown that the necessity to compensate losses of plasma on the surface of microparticles may cause modification of the axial electric field inside the microparticle suspensions. For example, inside a suspension of 6.86-μm-diameter microparticles freely drifting inside a unipolar DC discharge in neon with 1 mA current at 0.6 mbar, the axial electric field can vary up to a factor of four [32]. In the experiment of Ref. [32], such a gradient in the axial electric field revealed itself in the longitudinal gradient of plasma emission.
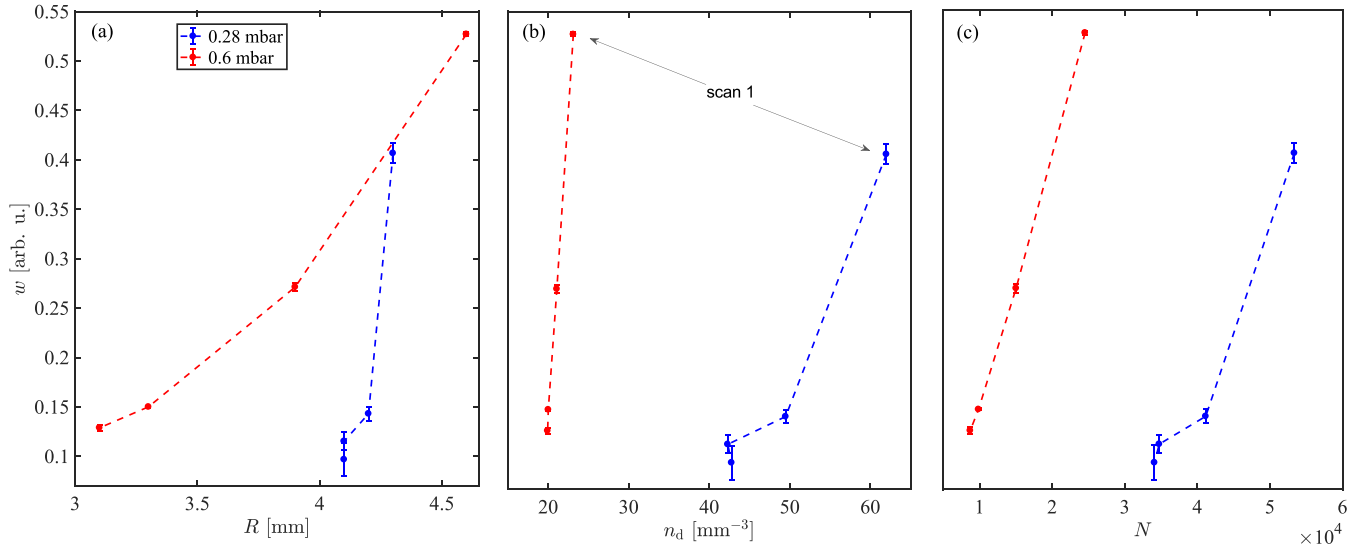
FIG. 4. Dependence of the average SLC length spectrum decay rate w on (a) the radius of the microparticle suspension R, (b) average number density of microparticles n_d, and (c) total number of detected microparticles N. Points with largest w correspond to the first scan [as shown in panel (b)]. Clear increase of w with all the three quantities is observed, suggesting the importance of microparticle-plasma interactions. For a pressure of 0.6 mbar, the error bars are within the point markers.

Experimentally observed slow drift of a microparticle suspension may therefore cause the change of the electric field in the discharge region in the field of view of the cameras. The quadrupole term of the microparticle interaction potential $\phi_Q \sim M^2$ [Eq. (2)] is very sensitive to the value of the electric field driving the flow.

In an attempt to detect the possible changes of the axial electric field, we analyzed the images of the PK-4 glow camera. Although the PK-4 glow kaleidoscope is designed for neon [1], the 703.2 nm channel partially transmits also the 706.7 nm spectral line of argon, which was used as a working gas in the present work. We were, however, unable to detect any difference in the distribution of the axial emission profile between the periods corresponding to the scans. The changes might be obscured by the line-of-sight averaging as well as by the low intensity of the signal and, consequently, large noise.

We should also note that the electric field in a DC discharge is subject to large fluctuations due to running striations with the frequencies in the kHz or tens of kHz range [33]. For PK-4, this problem was investigated in Ref. [34]. The values of the electric field given in Ref. [32] are averaged over those fluctuations. However, since $\phi_Q \sim M^2$, the rms value of the electric field, which may even be more sensitive to the local parameters of the suspension than its average value, is relevant for the interparticle attraction [34].

Nevertheless, the importance of microparticle-plasma interactions in the formation of the string order in PK-4 still remains a hypothesis. Long (minutes) intervals between the scans do not allow us to completely exclude such factors as contamination of the plasma or sputtering of the microparticles. Sputtering rates of the order of 0.05 μm/min were reported for the DC discharges [35,36]. It also cannot be excluded that the suspension might naturally evolve on the timescale of minutes [37] even at constant background plasma conditions. Uncontrolled drift and shape of the microparticle suspensions did not allow us to always vary the thickness of the suspension in a large enough range: For 0.6 mbar, the faster drift causes larger range of R [Fig. 4(a)]. In a dedicated future experiment, we will be able to vary the thickness of the microparticle suspension by injecting different amounts of microparticles into the plasma. The scans performed immediately after the trapping of microparticles will be compared. These experiments should allow us to make a final conclusion on the role of microparticle-plasma interactions in the formation of the string order in PK-4 and complex plasmas in general.

VI. CONCLUSION

Long-term evolution of the 3D structure of the microparticle suspensions in a polarity-switched DC discharge plasma of the PK-4 laboratory was investigated using the pair correlations and the SLC length spectrum. The 3D structure was determined in four consecutive tomographic scans of the microparticle suspension taken with two-minute intervals. The average decay rate of the SLC length spectrum was used as a measure of string order. It was shown that the improvement of the string order from scan to scan is accompanied by the decrease of the thickness of the suspension, microparticle number density, and total amount of the microparticles in the field of view. These structural changes occurred at constant discharge current, polarity switching frequency, and duty cycle as well as constant working gas pressure and therefore may be attributed to the local changes in the plasma caused by the redistribution of the microparticle component. For the final conclusion, however, further experiments are required to exclude possibilities of intrinsic long-term evolution, effects of plasma contamination and sputtering of microparticles between the scans.

[1] M. Y. Pustylnik, M. A. Fink, V. Nosenko, T. Antonova, T. Hagl, H. M. Thomas, A. V. Zobnin, A. M. Lipaev, A. D. Usachev, V. I. Molotkov, O. F. Petrov, V. E. Fortov, C. Rau, C. Deysenroth, S. Albrecht, M. Kretschmer, M. H. Thoma, G. E. Morfill, R. Seurig, A. Stettner *et al.*, Rev. Sci. Instrum. **87**, 093505 (2016).

[2] A. P. Nefedov, G. E. Morfill, V. E. Fortov, H. M. Thomas, H. Rothermel, T. Hagl, A. V. Ivlev, M. Zuzic, B. A. Klumov, A. M. Lipaev, V. I. Molotkov, O. F. Petrov, Y. P. Gidzenko, S. K. Krikalev, W. Shepherd, A. I. Ivanov, M. Roth, H. Binnenbruck, J. A. Goree, and Y. P. Semenov, New J. Phys. **5**, 33 (2003).

[3] H. M. Thomas, G. E. Morfill, V. E. Fortov, A. V. Ivlev, V. I. Molotkov, A. M. Lipaev, T. Hagl, H. Rothermel, S. A. Khrapak, R. K. Sütterlin, M. Rubin-Zuzic, O. F. Petrov, V. I. Tokarev, and S. K. Krikalev, New J. Phys. **10**, 033036 (2008).

[4] V. E. Fortov, A. V. Ivlev, S. A. Khrapak, A. G. Khrapak, and G. E. Morfill, Phys. Rep. **421**, 1 (2005).

[5] G. E. Morfill and A. V. Ivlev, Rev. Mod. Phys. **81**, 1353 (2009).

[6] V. Fortov and G. Morfill, *Complex and Dusty Plasmas: From Laboratory to Space* (CRC Press, Boca Raton, 2009).

[7] A. Ivlev, H. Löwen, G. Morfill, and C. Royall, *Complex Plasmas and Colloidal Dispersions: Particle-Resolved Studies of Classical Liquids and Solids* (World Scientific, Hackensack, 2012).

[8] S. Mitic, B. A. Klumov, U. Konopka, M. H. Thoma, and G. E. Morfill, Phys. Rev. Lett. **101**, 125002 (2008).

[9] B. A. Klumov, Phys. Usp. **53**, 1053 (2010).

[10] B. Klumov, P. Huber, S. Vladimirov, H. Thomas, A. Ivlev, G. Morfill, V. Fortov, A. Lipaev, and V. Molotkov, Plasma Phys. Control. Fusion **51**, 124028 (2009).

[11] B. Klumov, G. Joyce, C. Räth, P. Huber, H. Thomas, G. E. Morfill, V. Molotkov, and V. Fortov, Europhys. Lett. **92**, 15003 (2010).

[12] S. A. Khrapak, B. A. Klumov, P. Huber, V. I. Molotkov, A. M. Lipaev, V. N. Naumkin, H. M. Thomas, A. V. Ivlev, G. E. Morfill, O. F. Petrov, V. E. Fortov, Y. Malentschenko, and S. Volkov, Phys. Rev. Lett. **106**, 205001 (2011).

[13] S. A. Khrapak, B. A. Klumov, P. Huber, V. I. Molotkov, A. M. Lipaev, V. N. Naumkin, A. V. Ivlev, H. M. Thomas, M. Schwabe, G. E. Morfill, O. F. Petrov, V. E. Fortov, Y. Malentschenko, and S. Volkov, Phys. Rev. E **85**, 066407 (2012).

[14] D. Samsonov, G. E. Morfill, H. M. Thomas, T. Hagl, H. Rothermel, V. E. Fortov, A. M. Lipaev, V. I. Molotkov, A. P. Nefedov, O. F. Petrov, A. Ivanov, and S. K. Krikalev, Phys. Rev. E **67**, 036404 (2003).

[15] C.-R. Du, R. K. Sütterlin, A. V. Ivlev, H. M. Thomas, and G. E. Morfill, Europhys. Lett. **99**, 45001 (2012).

[16] C.-R. Du, R. K. Sütterlin, K. Jiang, C. Räth, A. V. Ivlev, S. A. Khrapak, M. Schwabe, H. M. Thomas, V. E. Fortov, A. M. Lipaev, V. I. Molotkov, O. F. Petrov, Y. Malentschenko, F. Yurtschichin, Y. Lonchakov, and G. E. Morfill, New J. Phys. **14**, 073058 (2012).

[17] V. Nosenko, M. Pustylnik, M. Rubin-Zuzic, A. M. Lipaev, A. V. Zobnin, A. D. Usachev, H. M. Thomas, M. H. Thoma, V. E. Fortov, O. Kononenko, and A. Ovchinin, Phys. Rev. Research **2**, 033404 (2020).

[18] A. V. Ivlev, G. E. Morfill, H. M. Thomas, C. Räth, G. Joyce, P. Huber, R. Kompaneets, V. E. Fortov, A. M. Lipaev, V. I. Molotkov, T. Reiter, M. Turin, and P. Vinogradov, Phys. Rev. Lett. **100**, 095003 (2008).

[19] A. V. Ivlev, M. H. Thoma, C. Räth, G. Joyce, and G. E. Morfill, Phys. Rev. Lett. **106**, 155001 (2011).

[20] M. Y. Pustylnik, B. Klumov, M. Rubin-Zuzic, A. M. Lipaev, V. Nosenko, D. Erdle, A. D. Usachev, A. V. Zobnin, V. I. Molotkov, G. Joyce, H. M. Thomas, M. H. Thoma, O. F. Petrov, V. E. Fortov, and O. Kononenko, Phys. Rev. Research **2**, 033314 (2020).

[21] M. Schwabe, S. A. Khrapak, S. K. Zhdanov, M. Y. Pustylnik, C. Räth, M. Fink, M. Kretschmer, A. M. Lipaev, V. I. Molotkov, A. S. Schmitz, M. H. Thoma, A. D. Usachev, A. V. Zobnin, G. I. Padalka, V. E. Fortov, O. F. Petrov, and H. M. Thomas, New J. Phys. **22**, 083079 (2020).

[22] T. J. Chen, R. N. Zitter, and R. Tao, Phys. Rev. Lett. **68**, 2555 (1992).

[23] U. Dassanayake, S. Fraden, and A. van Blaaderen, J. Chem. Phys. **112**, 3851 (2000).

[24] O. Ashour, C. A. Rogers, and W. Kordonsky, J. Intell. Mater. Syst. Struct. **7**, 123 (1996).

[25] J. de Vicente, D. J. Klingenberg, and R. Hidalgo-Alvarez, Soft Matter **7**, 3701 (2011).

[26] S. Mitic, B. A. Klumov, S. A. Khrapak, and G. E. Morfill, Phys. Plasmas **20**, 043701 (2013).

[27] S. Jaiswal, M. Y. Pustylnik, S. Zhdanov, H. M. Thomas, A. M. Lipaev, A. D. Usachev, V. I. Molotkov, V. E. Fortov, M. H. Thoma, and O. V. Novitskii, Phys. Plasmas **25**, 083705 (2018).

[28] R. Kompaneets, Phys. Plasmas **14**, 052108 (2007).

[29] G. I. Sukhinin, A. V. Fedoseev, M. V. Salnikov, S. N. Antipov, O. F. Petrov, and V. E. Fortov, Europhys. Lett. **103**, 35001 (2013).

[30] A. V. Fedoseev, G. I. Sukhinin, M. K. Dosbolayev, and T. S. Ramazanov, Phys. Rev. E **92**, 023106 (2015).

[31] M. Y. Pustylnik, I. L. Semenov, E. Zähringer, and H. M. Thomas, Phys. Rev. E **96**, 033203 (2017).

[32] A. V. Zobnin, A. D. Usachev, O. F. Petrov, V. E. Fortov, M. H. Thoma, and M. A. Fink, Phys. Plasmas **25**, 033702 (2018).

[33] P. S. Landa, N. A. Miskinova, and Y. V. Ponomarev, Sov. Phys. Usp. **23**, 813 (1980).

[34] P. Hartmann, M. Rosenberg, Z. Juhasz, L. S. Matthews, D. L. Sanford, K. Vermillion, J. Carmona-Reyes, and T. W. Hyde, Plasma Sources Sci. Technol. **29**, 115014 (2020).

[35] M. A. Ermolenko, E. S. Dzlieva, V. Y. Karasev, S. I. Pavlov, V. A. Polishchuk, and A. P. Gorbenko, Tech. Phys. Lett. **41**, 1199 (2015).

[36] V. Y. Karasev, E. S. Dzlieva, A. P. Gorbenko, I. C. Mashek, V. A. Polishchuk, and I. I. Mironova, Tech. Phys. **62**, 496 (2017).

[37] PK-3 Plus Team (private communication).